

Journal of Materials Chemistry A

Materials for energy and sustainability

Accepted Manuscript

This article can be cited before page numbers have been issued, to do this please use: J. Cho, D. H. Kim, M. W. Noh, H. Kim, H. Oh, P. Lee, S. Yoon, W. Won, Y. Park, U. Lee and C. H. Choi, *J. Mater. Chem. A*, 2024, DOI: 10.1039/D4TA02755H.



This is an Accepted Manuscript, which has been through the Royal Society of Chemistry peer review process and has been accepted for publication.

Accepted Manuscripts are published online shortly after acceptance, before technical editing, formatting and proof reading. Using this free service, authors can make their results available to the community, in citable form, before we publish the edited article. We will replace this Accepted Manuscript with the edited and formatted Advance Article as soon as it is available.

You can find more information about Accepted Manuscripts in the [Information for Authors](#).

Please note that technical editing may introduce minor changes to the text and/or graphics, which may alter content. The journal's standard [Terms & Conditions](#) and the [Ethical guidelines](#) still apply. In no event shall the Royal Society of Chemistry be held responsible for any errors or omissions in this Accepted Manuscript or any consequences arising from the use of any information it contains.

ARTICLE

Dissolution of Ti porous transport layer in proton exchange membrane water electrolyzer

Junsic Cho,^{a,†} Dong Hyun Kim,^{a,†} Min Wook Noh,^a Haesol Kim,^a Hong-Gyun Oh,^b Pilyoung Lee,^c Soobin Yoon,^c Wangyun Won,^d Young-June Park,^{c*} Ung Lee^{e,f,g*} and Chang Hyuck Choi^{a,h*}Received 00th January 20xx,
Accepted 00th January 20xx

DOI: 10.1039/x0xx00000x

Titanium porous transport layer (PTL) is a key component in the proton exchange membrane water electrolyzer (PEMWE), facilitating efficient water supply into the catalyst layer while rapidly removing oxygen bubbles. However, in the highly anodic operating environment of PEMWE, Ti PTL suffers from degradation, limiting the lifetime of the device. To gain deeper insights into Ti PTL degradation, here we monitor the potential/time-resolved Ti dissolution rates by coupling PEMWE with online inductively coupled plasma-mass spectrometry (ICP-MS). The results show that the dissolution of Ti PTL is a complex and dynamic (electro)chemical event. Initiated by decreased interfacial pH (even at pH <1) due to proton accumulation during PEMWE operation, Ti dissolution intensifies with increasing bias potential. However, the dissolved Ti ions are simultaneously hydrolyzed, forming surface Ti oxides that slow down the dissolution rate. Coating the Ti PTL surface with Pt and IrO₂ effectively reduces Ti dissolution, albeit at a higher cost, but they are also susceptible to dissolution during operation. Interestingly, the dissolution profiles of Pt and IrO₂ deposited on Ti PTL differ significantly from their conventional behavior, which requires further investigation for reliable prediction and optimization of new PTL designs for practical implementation in PEMWE.

Introduction

In the quest for a sustainable, carbon-neutral future, there is a growing energy paradigm shift away from polluting fossil fuels toward a cleaner and more sustainable society.¹ At the heart of this new energy economy is green hydrogen.² A critical technology driving this transformation is the proton exchange membrane water electrolyzer (PEMWE),¹ which produces hydrogen gas from abundant water with minimal, or ideally zero, greenhouse gas emissions. PEMWE has demonstrated promising performance and rapid response to fluctuations in power supply, making it well-suited for integration with renewable energy sources. However, its harsh operating conditions (>2 V, temperature of 60–80 °C, and acidic

environments) limit the choice of materials library that can be used in PEMWE, as they must have high corrosion resistance.^{3,4}

Titanium offers relatively high corrosion resistance under such conditions, with high electrical conductivity and mechanical strength.⁵ Therefore, in addition to the bipolar plates, the porous transport layer (PTL), an essential component of PEMWE for efficiently supplying the water flow to the catalyst layer while facilitating the removal of oxygen bubbles, is typically made of metallic Ti.^{6–10} Its remarkable corrosion resistance is due to the formation of a stable protective oxide layer (generally TiO₂) on its surface when exposed to air or water. This layer is extremely adherent and has the ability to repair itself if damaged, providing robust protection against various corrosive environments. However, the poor electrical conductivity of the protective layer leads to an increase in the ohmic resistance between the PTL and other components of the PEMWE, which can significantly deteriorate the energy efficiency of the PEMWE.^{11,12} This drawback has prompted several strategies to ensure durable operation, including optimizing the PTL morphology and coating the metallic Ti surface with thin layers of noble metals (e.g., Pt, Ir, etc.).¹³

It should be noted, however, that titanium and even noble metals used to protect Ti are not completely immune to corrosion. Using a scanning flow cell (SFC) coupled to an inductively coupled plasma-mass spectrometer (ICP-MS), several research groups have investigated the potential-resolved electrochemical stability of Ti-containing mixed oxide catalysts (e.g., Ir-TiO_x,^{14–16} Ir/CuTiO_x,¹⁷ and RuIr-TiO_x¹⁸) in a 0.1 M HClO₄ electrolyte. While these studies focused primarily on the dissolution of noble metal catalysts and the subsequent

^a Department of Chemistry, Pohang University of Science and Technology (POSTECH), Pohang 37673, Republic of Korea. E-mail: chchoi@postech.ac.kr

^b Global Sales Department, Shinsung C&T, Suwon 16648, Republic of Korea

^c Hydrogen and Fuel Cell Development Center, Hyundai Motor Group, Yongin 16891, Republic of Korea. E-mail: yjpark2935@hyundai.com

^d Department of Chemical and Biological Engineering, Korea University, 145, Seoul 02841, Republic of Korea

^e Clean Energy Research Center, Korea Institute of Science and Technology, Seoul 02792, Republic of Korea. E-mail: ulee@kist.re.kr

^f Green School, Korea University, 145 Anam-ro, Seongbuk-gu, Seoul 02841, Republic of Korea

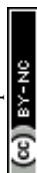
^g KIST Europe, Korea Institute of Science and Technology Europe, Campus E71, Saarbrücken 66123, Germany

^h Institute for Convergence Research and Education in Advanced Technology (I-CREATE), Yonsei University, Seoul 03722, Republic of Korea

*These authors contributed equally to this work.

†Electronic Supplementary Information (ESI) available. See

DOI: 10.1039/x0xx00000x



decline in their oxygen evolution reaction (OER) activity — and thus the results may not fully represent the behavior of Ti PTL in PEMWE — they showed appreciable Ti dissolution, following a trend similar to that of noble metal dissolution. Meanwhile, Rakousky *et al.* observed the presence of Ti^{n+} species at the cathode in the aged catalyst-coated membrane (CCM) after

>1000 h of conventional PEMWE operation (2 A cm^{-2} and $80 \text{ }^\circ\text{C}$).¹² Since the cathode in pristine CCM was free of Ti and this element was only present in the anode catalyst (a mixture of IrO_2 and TiO_2) and Ti PTL, Ti dissolution under PEMWE operation was clearly identified. In addition, Ti crossover from anode PTL to cathode was also observed in PEMWE for H_2O_2 synthesis,

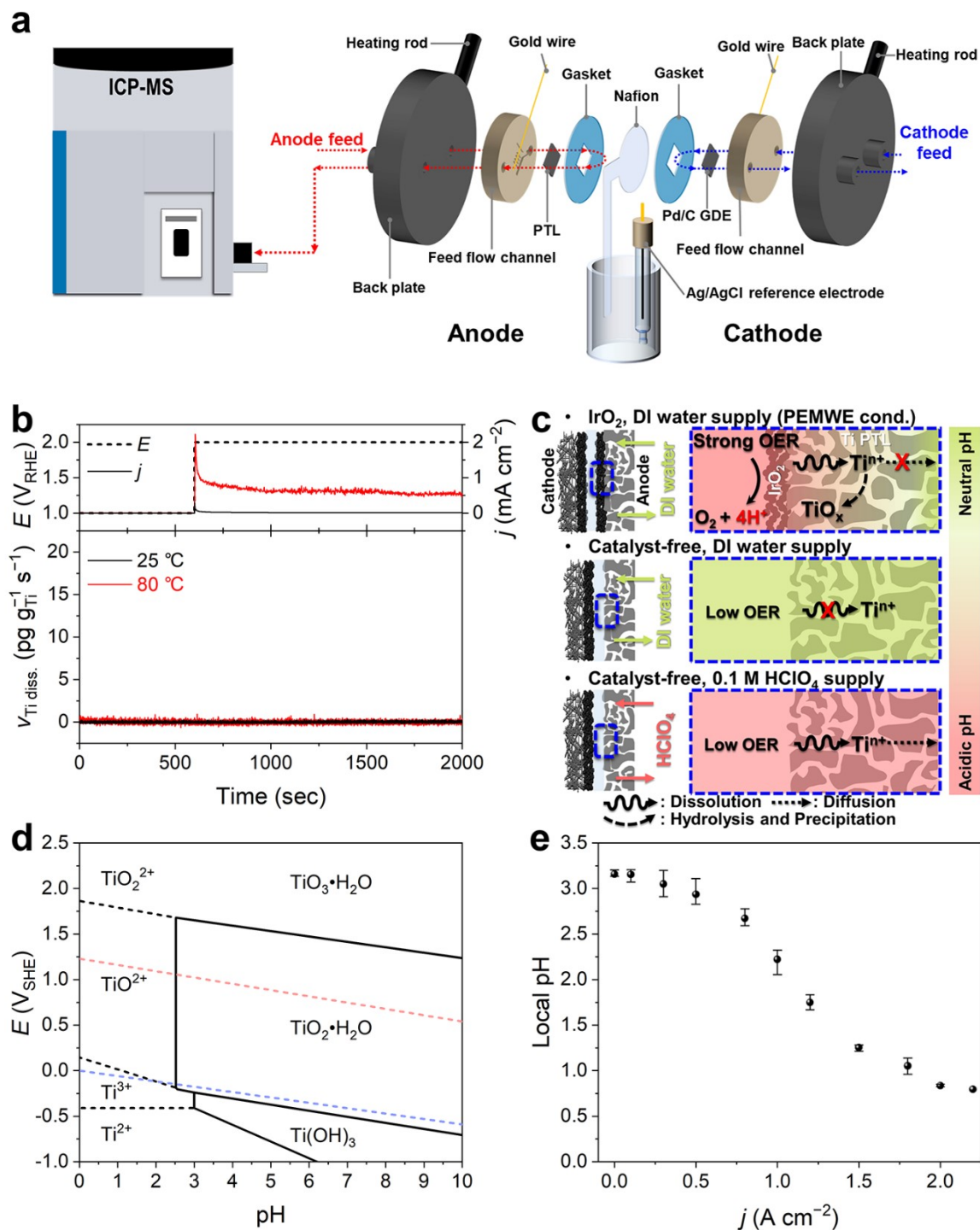


Fig. 1 (a) Schematic representation of the online PEMWE/ICP-MS setup. (b) Real-time Ti dissolution measured at a static potential of $2 V_{RHE}$ with a supply of O_2 -saturated DI water at 25 and $80 \text{ }^\circ\text{C}$. (c) Schematic representation of Ti dissolution behavior for three different operating conditions: PEMWE operation (*i.e.*, Ti PTL with catalyst layer and DI water supply) and our model systems of catalyst-free Ti PTL with DI water or 0.1 M HClO_4 supply. (d) Pourbaix diagram of Ti. (e) Estimated local pHs at the electrode-membrane interface measured at different current densities.



where Ti felt was used as PTL but the anode catalyst was only IrO_2 .¹⁹ Thus, the previous findings highlight the need for a deeper understanding of Ti PTL dissolution under PEMWE conditions in order to develop rational PTL designs and operation strategies to meet industrial requirements.

In this study, Ti PTL dissolution in PEMWE was studied using an online ICP-MS, which allowed potential/time-resolved and quantitative monitoring of the Ti dissolution rate during electrochemical operation. We clearly identified non-negligible Ti dissolution, the rate of which is strongly influenced by feedstock (or interfacial) pH and applied potential. On the other hand, dissolved Ti ions undergo hydrolysis and form Ti oxide passivation layer, which suppresses the Ti dissolution rate. We investigated this complex event, during which dissolution and redeposition processes dynamically compete, under various potential profiles on commercialized Ti PTLs with and without Pt and IrO_2 coating layers. Our findings highlight the necessity of similar or further modified diagnostics for better design and evaluation of PTLs to ensure their high durability during PEMWE operation.

Results and discussion

View Article Online

DOI: 10.1039/D4TA02755H

For the online monitoring of Ti dissolution from PTL, we coupled a PEMWE cell with ICP-MS (Fig. 1a). At the anode, Ti PTL without OER catalyst, typically $\text{Ir}(\text{O}_x)$, was used as the electrode. On the other hand, at the cathode, a Pd/C catalyst rather than conventional Pt/C, which was coated on the gas-diffusion layer (GDL), was employed. It is of note that these distinct configurations of electrodes were due to the elimination of any interferences of Ir or Pt dissolution from the conventional catalytic substances for accurate investigation on Pt/ IrO_2 -coated Ti PTLs that will be discussed later, and due to minimization of bubble formation that can disrupt stable operation of the online monitoring. The anode and cathode were separated by a Nafion membrane, which was extended out of the electrolyzer cell and connected with a saturated Ag/AgCl reference electrode. This unique cell configuration,²⁰ beyond the conventional two-electrode system, provided excellent experimental reproducibility and allowed us to accurately control and monitor the anode (or cathode) potential in the electrochemical device (Fig. S1). Heating rods were inserted into the back plates of the cell to heat the cell.

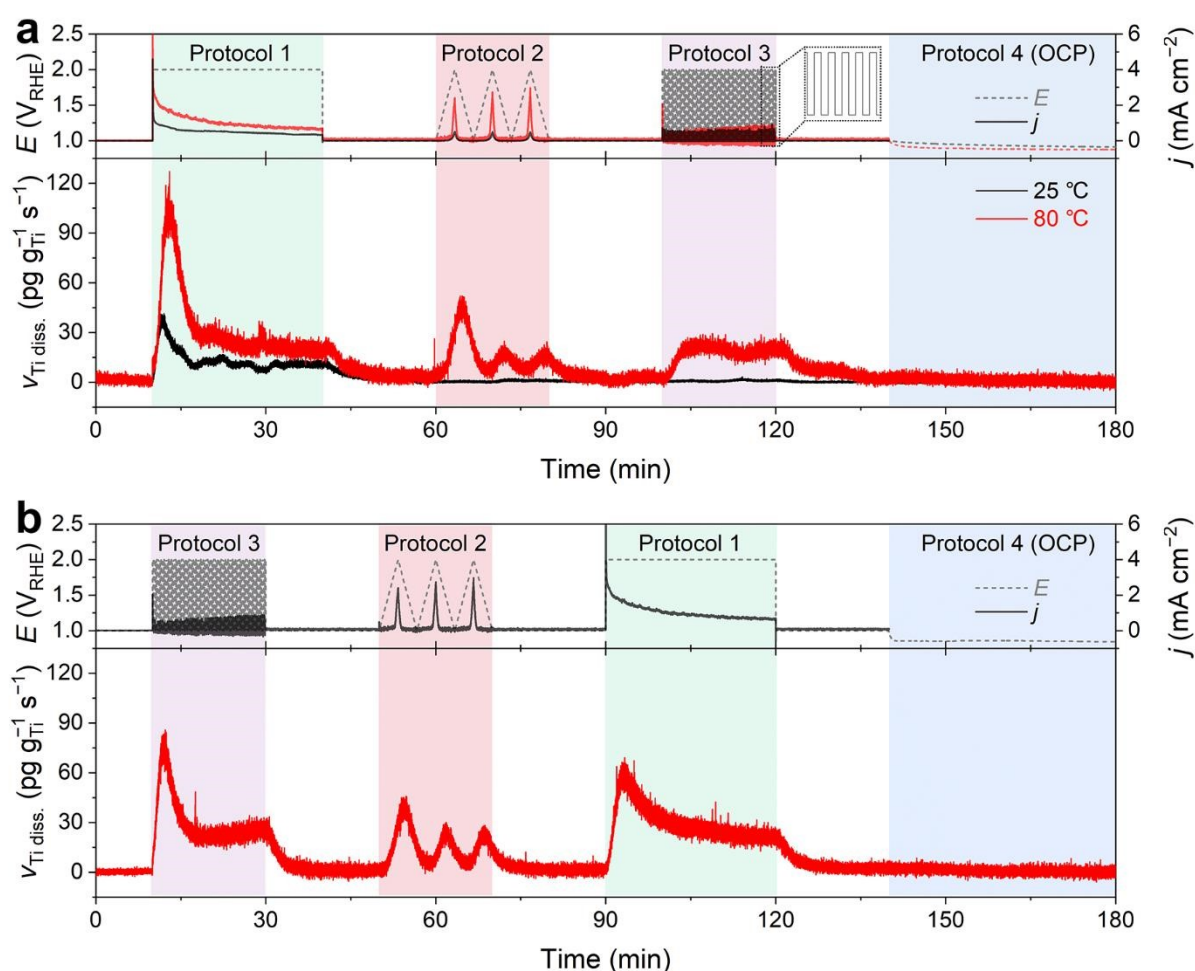


Fig. 2 Real-time dissolution profiles of Ti PTL measured during potential hold (Protocol 1), 3 cycles of CV (Protocol 2), and potential pulses (Protocol 3). For comparison, Ti dissolution was monitored in the order of (a) Protocols 1 → 2 → 3 at 25 and 80 °C and (b) Protocols 3 → 2 → 1 at 80 °C with a supply of O_2 -saturated 0.1 M HClO_4 feedstock. At the end of the measurements, the Ti PTL was not externally biased but rested at OCP (Protocol 4).



During the measurement, feedstock was supplied at a constant flow rate of 5 mL min⁻¹ on each electrode side, of which 400 μL min⁻¹ was introduced into the ICP-MS (see details in Experimental methods).

Ti dissolution was first investigated at 25 and 80 °C with a continuous flow of deionized (DI) water, typical feedstock for commercialized PEMWE, during the anode polarizations at 1 and 2 V vs. reversible hydrogen electrode (RHE; Fig. 1b), which are in relevant potential range for rest and OER operating potentials, respectively. However, at both temperatures, we found no discernible Ti dissolution during the operation. This result does not agree with previous findings that showed non-negligible Ti dissolution after PEMWE operation,^{12,21} thereby implying that our experimental conditions insufficiently reflect those in practical PEMWE.

We envisioned that this discrepancy primarily originated from different H₂O consumption and H⁺ production rates, leading to consequent differences in local pH at the PTL-electrolyte interface (Fig. 1c). In practical PEMWEs, ampere-order current density (*j*) is typically achieved for efficient evolution of O₂ gas. We also confirmed that our system also reached >2 A cm⁻² of *j* when using the IrO₂ catalyst layer (Fig. S2). This leads to considerable H⁺ production at the anode and its possible accumulation at the interface, lowering the interfacial pH.^{22,23} However, in our system, Ti PTL free from anode catalyst resulted in a marginal *j* less than 1 mA cm⁻² even at 2 V_{RHE} (Fig. 1b), thereby no considerable changes in the interfacial pH can be reasonably deduced. The importance of feedstock pH on the Ti dissolution can also be understood with the Pourbaix diagram of Ti (Fig. 1d), which shows that pH lower than approximately 2.5 is thermodynamically needed for the exergonic dissolution process of Ti to TiO₂⁺ or TiO₂²⁺ at potential above 1 V_{RHE}. It is of note that, at a given pH 7 of DI water, the most stabilized phase of Ti is solid TiO₂•H₂O or TiO₃•H₂O depending on the potential applied.²⁴

To confirm this hypothesis, *i.e.*, greater accumulation of H⁺ at the interface with increasing *j*, we estimated the current-dependent local pH changes using the method recently developed by Sauv   *et al.*,²⁵ which follows a quasi-equilibrium potential between hydrogen oxidation and reduction reactions on Pt and estimates the interfacial pH (Fig. S3). The result showed that even at zero current, the interface exhibited a slightly acidic nature (pH 3.2, Fig. 1e), due to the sulfonic acid group-terminated Nafion membrane.^{26,27} However, as the current increased, the pH decreased significantly, and it even reached below pH 1 when the *j* exceeded 1.8 A cm⁻². Therefore, for subsequent online ICP-MS experiments, we opted to use a 0.1 M HClO₄ solution instead of DI water as the feedstock. This choice was made to more accurately simulate the interfacial conditions of real PEMWE without an anode catalyst and to avoid any chemical decomposition and precipitation of dissolved Ti ions into solid TiO_x as they moved away from the diffusion layer before being analyzed by ICP-MS (Fig. 1c).

In this measurement, we monitored the dissolution rate of Ti in O₂-saturated 0.1 M HClO₄ during four consecutive potential protocols (Fig. 2). Protocol 1 entailed the potentiostatic operation of PEMWE, with a potential hold of the Ti PTL at 2

V_{RHE} for 30 min. Conversely, Protocols 2 and 3 involved potentiodynamic conditions, comprising three cyclic voltammograms (CVs) at a scan rate of 5 mV s⁻¹ and 60 cycles of potential pulses of 10 s each within a potential range of 1–2 V_{RHE}, respectively. Typically, the measurement was performed in the order of Protocols 1 → 2 → 3 (Fig. 2a), although the reverse order, Protocols 3 → 2 → 1 (Fig. 2b), was also evaluated. Protocol 4 was then implemented, which corresponded to potential rest, *i.e.*, open circuit potential (OCP), for 40 min. Before and after each protocol, the Ti PTL was polarized at 1 V_{RHE} to stabilize the ICP-MS signals.

In contrast to the results observed with DI water (Fig. 1b and Fig. S4), we observed significant Ti dissolution in the HClO₄ feedstock. At 25 °C, significant Ti dissolution rate was found in Protocol 1, but it was almost negligible in the following Protocols 2–4. On the other hand, at 80 °C, a practically more relevant temperature, much greater dissolution of Ti was

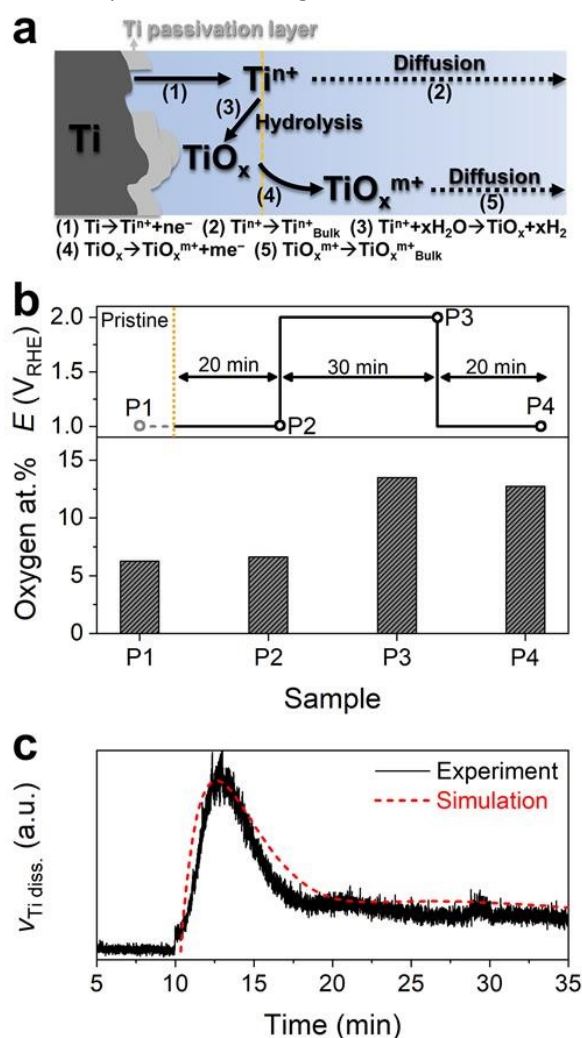


Fig. 3 (a) Schematic representation of the expected Ti PTL dissolution mechanism at highly anodic conditions. The reaction equation of each step is also shown. (b) Oxygen atomic percentages on Ti PTL before (P1; gray circle) and after specific potential application (P2, P3, and P4; black circles) in O₂-saturated 0.1 M HClO₄. Oxygen content was estimated by EDS analysis. (c) Comparison of experimental and simulated Ti dissolution profiles at 2 V_{RHE}.



observed in Protocols 1–3 (Fig. 2a). In addition, it is noteworthy that the Ti dissolution signals were observed in both anolyte and catholyte (Fig. S5). This result indicates the crossover of Ti ions from anode to cathode, which is consistent with previous results measured after long-term operation of PEMWE.¹² However, the Ti signal measured in the anolyte was approximately 6 times higher than that in the catholyte, suggesting that the diffusion of dissolved Ti ions from the anode to the cathode was relatively marginal under our experimental conditions. Therefore, the following investigations focused solely on the dissolution of Ti PTL in the anolyte at 80 °C.

In the standard protocol sequence (Fig. 2a), no perceptible Ti dissolution was detected at 1 V_{RHE} . However, at the initial potential jump to 2 V_{RHE} in Protocol 1, the Ti PTL exhibited substantial Ti dissolution of approximately $100 \text{ pg g}_{Ti}^{-1} \text{ s}^{-1}$. However, the intense Ti dissolution rapidly decreased within 500 seconds and stabilized at approximately $25 \text{ pg g}_{Ti}^{-1} \text{ s}^{-1}$ during the potential hold. Afterward, in Protocol 3, a consistent Ti dissolution rate was observed, quantitatively similar to the plateau observed in Protocol 1. However, the initial intense Ti dissolution, seen in Protocol 1, was not found in Protocol 3, while the Ti PTL underwent the same potential shift from 1 to 2 V_{RHE} and experienced this drastic potential change repeatedly.

On the other hand, in the reverse protocol sequence (Fig. 2b), the initially intense but subsequently attenuated Ti dissolution was also recorded in Protocol 3, when it preceded all other protocols. The same conclusion was reached when the potential excursion started with Protocol 2 (Fig. S6). Therefore, these results implied that the most intense Ti dissolution occurs at the initial potential transition from 1 to 2 V_{RHE} , but thereafter its dissolution rate becomes relatively mitigated regardless of either potentiostatic or pulsed operation at 2 V_{RHE} .

It is generally accepted that the Ti surface can be protected against corrosion by forming stable passivation films, e.g., Ti oxide or hydroxide, even in acidic environments.^{28,29} However, the intense Ti dissolution at the first potential transition from 1 to 2 V_{RHE} allowed us to consider either that the Ti PTL surface is not fully protected by the passivation film, but contains some pits or defective sites, or that the native passivation layer is only quasi-stable, resulting in considerable Ti dissolution from exposed metallic Ti and/or quasi-stable Ti passivation layer at the highly anodic condition of 2 V_{RHE} (Fig. 3a). Nevertheless, the subsequent exponential decay of the Ti dissolution rate implies the hydrolysis of dissolved Ti ions at the interface and the formation of a relatively stable or thicker passivation layer on the Ti PTL, as also explained in the literature.^{28–30} Scanning

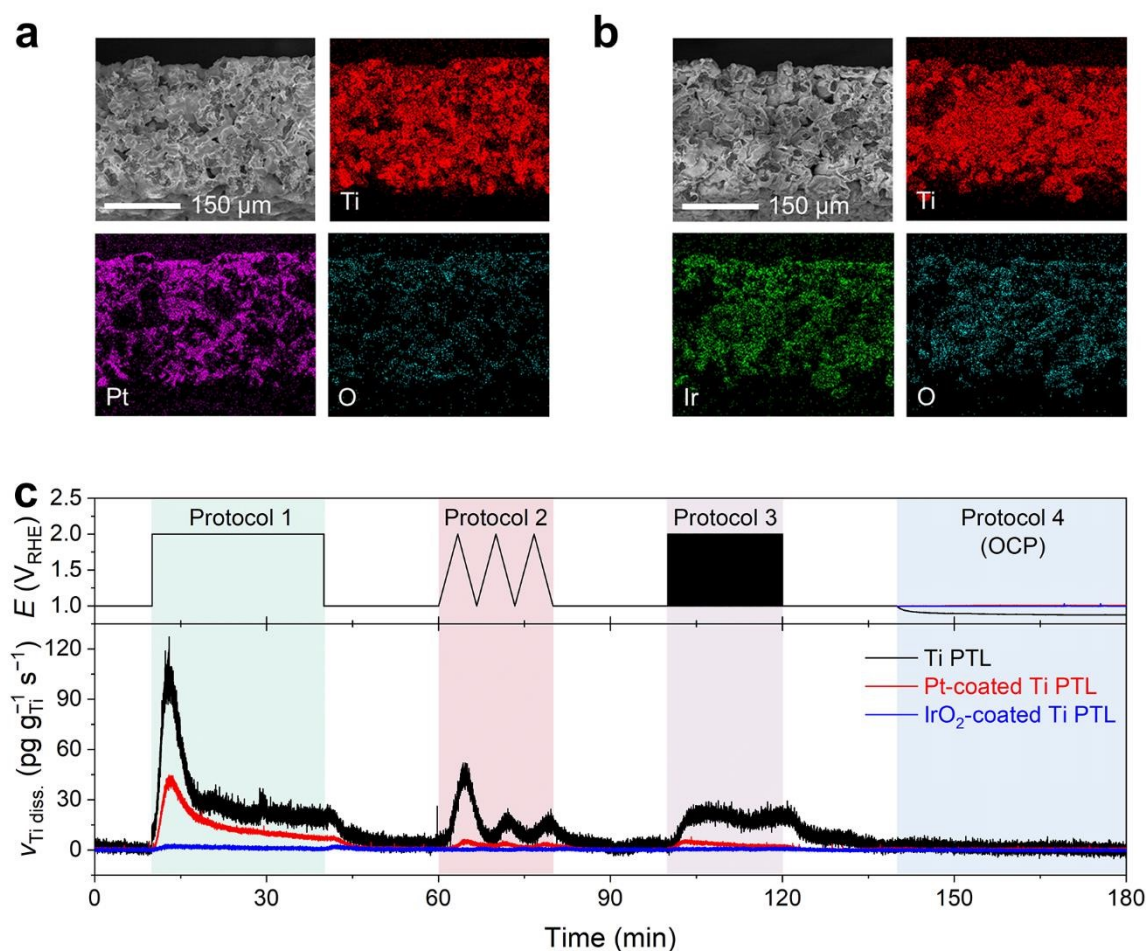


Fig. 4 Cross-sectional SEM and EDS results of (a) Pt- and (b) IrO_2 -coated Ti PTLs. (c) Real-time Ti dissolution profiles of Pt/ IrO_2 -coated Ti PTLs measured during potential hold (Protocol 1), 3 cycles of CV (Protocol 2), potential pulses (Protocol 3), and resting at OCP (Protocol 4) with a supply of O_2 -saturated 0.1 M HClO_4 feedstock.



electron microscopy (SEM) and energy-dispersive spectroscopy (EDS) of the Ti PTL revealed the increase in oxygen content after its polarization at 2 V_{RHE} , corroborating the formation of an additional passivation layer (Fig. 3b and Fig. S7). However, the marginal but consistent Ti dissolution during potential hold at 2 V_{RHE} and potential pulses between 1 and 2 V_{RHE} suggests that even the newly formed passivation layer may not be completely immune to corrosion, possibly because the thermodynamically most stable phase under such conditions is Ti ions (TiO_2^+ and TiO_2^{2+}) rather than solid Ti oxides. Computational modeling based upon the above simple mechanistic scenario toward Ti dissolution also successfully describes the trend of experimental results (Fig. 3c and Fig. S8), *i.e.*, initially intensive but subsequently marginal Ti dissolution, while more complex reactions may need to be further considered for more elaborate prediction. We note that Ti dissolution is likely electrochemical reactions,³¹ not chemical reactions,²⁹ since 1) no significant dissolution of Ti was observed at potential hold at 1 V_{RHE} before and after the protocols and during potential rest at OCP, and 2) the Ti dissolution rate increased with increasing potential as shown in Protocol 2.

After confirmation of possible Ti dissolution from bare Ti PTL under PEMWE-relevant operating conditions, we investigated the Ti dissolution behavior of Ti PTL onto which thin protecting layers of Pt and IrO_2 were coated. These modified Ti PTLs are commonly utilized in PEMWE to mitigate the formation of Ti oxide layers and consequently suppress the increase in contact resistance between the catalyst layer and the PTL.^{12,32-35} In this study, we employed commercially available Pt- and IrO_2 -coated

Ti PTLs, fabricated on identical Ti PTL substrates as those investigated in Fig. 2. SEM and EDS studies confirmed homogeneous dispersion of Pt and IrO_2 over the Ti PTLs (Fig. 4a and Fig. 4b), thickness of which were approximately 100 and 350 nm (Fig. S9), respectively.

Online ICP-MS results on Pt- and IrO_2 -coated Ti PTLs revealed a considerably reduced Ti dissolution rate compared to bare Ti PTL (Fig. 4c and see Fig. S10 for corresponding current densities). The total Ti dissolution amounts during the protocols were 125 $ng\ g_{Ti}^{-1}$ for bare Ti PTL, while Pt- and IrO_2 -coated Ti PTLs recorded only 39 and 4 $ng\ g_{Ti}^{-1}$, respectively. Despite the effective protection provided by the IrO_2 layer against Ti dissolution in our case, direct comparison between Pt- and IrO_2 -coated Ti PTLs and subsequent discussions on identifying the better protective layer may be less informative, as these modified Ti PTLs exhibit considerable differences in surface morphology (*e.g.*, thickness of the protective layer; Fig. S9) and noble metal content (Table S1). More case studies with Pt/ IrO_2 /or other protecting layer-coated Ti PTLs will be required to figure out optimal composition and morphology of the protecting layer. However, at the very least, our results clearly demonstrate that the surface coating strategy is beneficial in mitigating undesirable Ti dissolution from Ti PTLs during PEMWE operation, in addition to the well-known electrical conductivity enhancement.

However, our next question then oriented towards the stability of the protecting layers during the operation, since even noble Pt and IrO_2 are not immune against corrosion at such highly anodic environments.^{14-18,35-39}

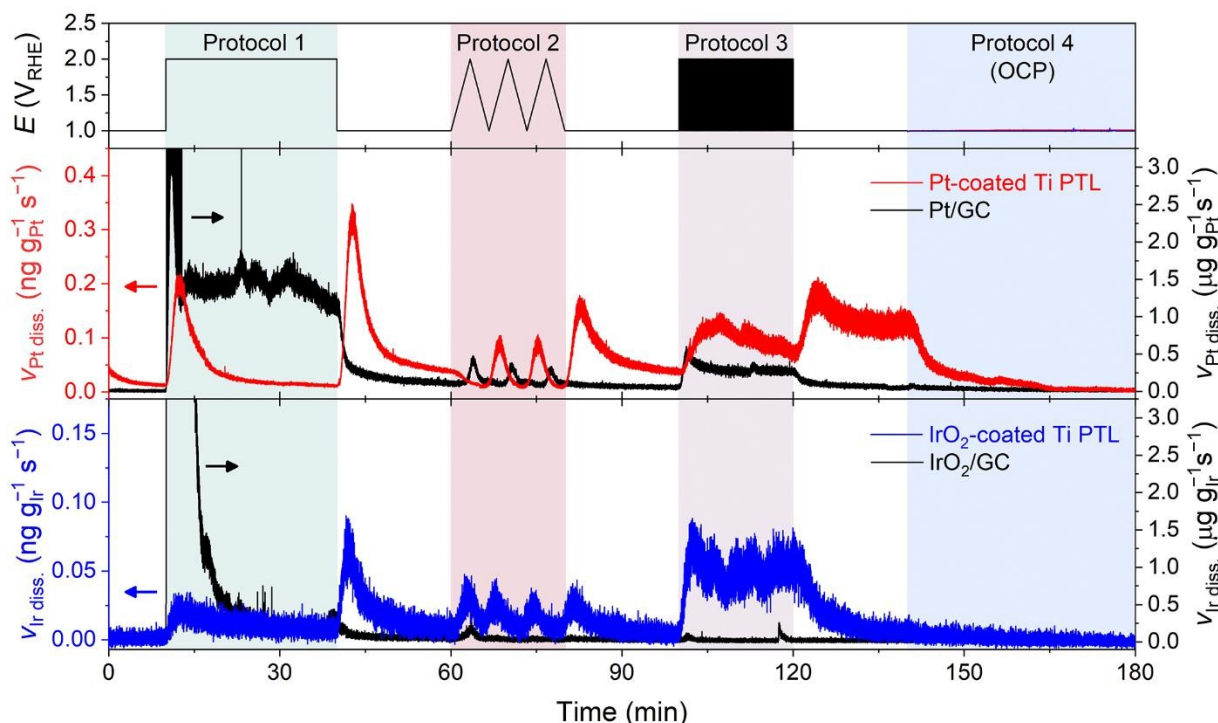


Fig. 5 Real-time dissolution profiles of Pt and Ir from Pt/ IrO_2 -coated Ti PTLs measured during potential hold (Protocol 1), 3 cycles of CV (Protocol 2), potential pulses (Protocol 3), and resting at OCP (Protocol 4) with a supply of O_2 -saturated 0.1 M $HClO_4$ feedstock. For comparison, dissolution profiles of commercially available Pt and IrO_2 nanoparticles deposited on a GC electrode were measured using an electrochemical flow cell at 25 °C.



Fig. 5 displays Pt and Ir dissolution profiles measured upon the modified Ti PTLs during Protocols 1–4 (see Fig. S10 for corresponding current densities). The results showed non-negligible dissolution of both protecting layers during the potential protocols. For the Pt-coated Ti PTL, Pt dissolution was found during potentiodynamic operation between 1 and 2 V_{RHE} , but interestingly, a significant Pt dissolution rate was also recorded during the potential hold at 1 V_{RHE} that followed the end of each protocol. It is noteworthy that Pt dissolution profile was different from that of conventional Pt particles deposited on a glassy carbon (GC) electrode, for which no considerable Pt dissolution was identified during the potential hold at 1 V_{RHE} . Indeed, for the IrO₂-coated Ti PTL, Ir dissolution occurred mainly during potentiodynamic operation, *i.e.*, beginning and end of Protocol 1 and during Protocols 2 and 3, while conventional IrO₂ showed much less Ir dissolution throughout the measurement except at the beginning of Protocol 1. Such fully different dissolution behaviors of Pt and IrO₂ in Ti PTLs, compared to conventional Pt and IrO₂, thus emphasize that the identity of the supporting electrode or substrate strongly influences the stability of Pt and IrO₂, as also pointed out recently by Zlatar *et al.*⁴⁰

Conclusions

In summary, we have investigated the dissolution of Ti PTLs in PEMWE by integrating online ICP-MS. We have shown that Ti dissolution occurs when the potential exceeds 1 V_{RHE} under both potentiostatic and potentiodynamic conditions. It is important to note, however, that our use of acidic 0.1 M HClO₄ feedstock may exaggerate Ti dissolution rates compared to practical PEMWE operations, which typically use neutral DI water. In practical settings, neutral DI water facilitates rapid hydrolysis of dissolved Ti ions, resulting in the precipitation of TiO_x and preventing the escape of Ti ions into the bulk feedstock (Fig. 1c). On the other hand, the use of 0.1 M HClO₄ also places the entire Ti PTL in an acidic environment, which can cause the entire PTL surface to corrode. Despite this limitation, even limited Ti dissolution at the electrode-membrane interface, a region that can become highly acidic during high current operations, could significantly degrade PEMWE performance. In more detail, dissolved Ti ions can precipitate on the anode and cathode as TiO_x, blocking the active surface of catalyst layers and reducing the electrochemically active surface area.⁴¹ Since TiO_x is an insulator, its accumulation can also lead to loss of electrical contact with active catalytic entities.^{11,12} Furthermore, the possible retention of dissolved Ti cations on the membrane through strong electrostatic interaction with anionic functional groups (*e.g.*, $-\text{SO}_3^-$ in Nafion) can hinder efficient proton transport and reduce cell performance.^{42,43} While protective layers on Ti PTLs, *i.e.*, Pt and IrO₂, can mitigate Ti dissolution to some extent, they can also dissolve under highly anodic conditions, and their dissolution behavior is significantly different from that of conventional Pt and IrO₂. This discrepancy thus highlights the critical importance of stability measurements directly on practically relevant electrode materials, rather than on well-understood and relatively simple

model substances, for accurate evaluation of their stability. In addition, while we have investigated three commercialized Ti PTLs in this study, a similar approach can be extended to other PTL electrodes with different protective layer loadings, morphologies, fabrication methods, etc., which may affect the dissolution rates of Ti and protective layers.^{44,45} Therefore, more comprehensive studies are needed to deepen our understanding and ultimately establish a better design of new Ti PTLs. Our results and the analytical platform used in this study lay the groundwork for such future research.

Experimental methods

Online ICP-MS measurements

The anode was commercial Ti PTL or Pt-/IrO₂-modified Ti PTL, all provided by Shinsung C&T. The PTLs were tailored to 0.36 cm² (0.6 cm × 0.6 cm) and directly introduced into the PEMWE without any OER catalysts. On the other hand, the cathode was a GDL (0.36 cm²), on which Pd/C (20 wt.% Pd, Sigma-Aldrich) was spray-coated with a target loading of 1 mg_{cat} cm⁻². To prepare the GDL, a highly hydrophobic carbon mesoporous layer (MPL) was deposited on a carbon paper (MGL280, AvCarb[®]) by spraying an ink, prepared by dispersing 100 mg of Ketjen black EC-300J (KB) and 200 mg of polytetrafluoroethylene (PTFE; 60 wt.%, Sigma-Aldrich) in 20 mL of isopropyl alcohol (99.5%, Sigma-Aldrich). The KB content in the MPL was adjusted to 2 mg cm⁻². The carbon paper was then sequentially heat-treated at 240 and 340 °C under an Ar flow for 30 min each.

Online metal dissolution was analyzed by ICP-MS (iCAP RQ, Thermo-Fisher Scientific) coupled to a homemade PEMWE (Fig. 1a), which verified comparable performance to other commercial PEMWE when using commercial membrane electrode assembly (MEA; Boyaz energy; anode of 4 mg cm⁻² IrO₂ and cathode of 0.5 mg_{Pt} cm⁻² Pt/C) (Fig. S2). The anode and cathode were separated by a Nafion 115 membrane (DuPont), which was extended from the PEMWE and connected to a saturated Ag/AgCl reference electrode to control the bias potential using a potentiostat (VMP3, Bio-Logic Science Inc.).²⁰ To avoid an unwanted Ti dissolution from a conventional Ti bipolar plate, feed flow channels were fabricated with polyether ether ketone (PEEK). Since the PEEK is an electrical insulator, an Au wire was connected to each electrode to provide electrical contact. All these compartments were assembled in the following order — back plate, flow channel, Au wire, Ti PTL, gasket, Nafion, gasket, Pd/C GDE, Au wire, flow channel, and back plate (Fig. 1a) — and then tightened with six bolts to a torque of 18 Nm. Heating rods were inserted into the back plates of the PEMWE to control cell temperature, and ICP-MS studies were performed at 25 and 80 °C.

The feedstock was either O₂-saturated DI water (>18.2 MΩ, Arium[®] Pro, Sartorius) or 0.1 M HClO₄ (diluted from 70% HClO₄, Sigma-Aldrich), which flowed through each PEEK flow channel at a flow rate of 5 mL min⁻¹ using a peristaltic pump (LEPP-150L, Labscitech). Prior to introduction of the feedstock into the ICP-MS, 400 μL min⁻¹ of the outflow was separated and mixed with 0.5 M HNO₃ containing 5 ppb ¹⁸⁷Re as an internal standard at a



1:1 mixing ratio using a Y-connector. Online metal dissolution was estimated from the ratio of metal ions (^{48}Ti , ^{193}Ir , and ^{195}Pt) to ^{187}Re signals during electrochemical measurements.

In control experiments, the dissolution of Pt and IrO₂ nanoparticles was investigated at 25 °C using a homemade electrochemical flow cell, which was used in our previous work.⁴⁶ Briefly, the cell consisted of a U-shaped channel (1 mm diameter) and two openings (3 mm diameter). On one opening side, a mirror-polished 3 mm GC electrode (002012, ALS) was introduced as a working electrode, on which 50 μg cm⁻² of Pt black (HiSPEC 1000, Alfa Aesar) or IrO₂ powder (Alfa Aesar) was deposited by drop-casting of an ink, prepared by dispersing 10 mg of Pt black or IrO₂ powder in a mixed solution of DI water (5,894 μL), isopropyl alcohol (1,079 μL), and 5 wt.% Nafion solution (100 μL). On the other opening side, a 3 mm Teflon tube sealed at one end with a PTFE membrane (WP-020-80, Sumitomo Electric Ind., Ltd.) was brought up to the working electrode surface to extract the evolved gases by vacuum. The counter electrode was a graphite rod separated from the electrolyte by a Nafion 115 membrane. The reference electrode was a saturated Ag/AgCl electrode connected directly to the electrolyte outlet.

Local pH measurements

The local pH change at the anode was measured by a method recently developed by Sauv  *et al.*,²⁵ which monitors the OCP decay transient (potential of the H₂/H⁺ equilibrium) on Pt. Our homemade PEMWE was used as the electrochemical platform, but a commercial Pt/C MEA (Boyaz energy) was installed. The MEA consisted of a Nafion 115 membrane, and Pt/C was deposited on both sides of the membrane with a loading of 0.5 mg_{Pt} cm⁻². A GDL and a Pt-coated Ti PTL were attached to the anode and cathode sides, respectively. H₂ gas, humidified at 50 °C, was introduced into the anode side at a flow rate of 200 sccm using a mass flow controller (M3030VA with LTI1000 readout box, LineTech), and Ar-saturated DI water was introduced into the cathode side at a flow rate of 5 mL min⁻¹. After stabilization of the potential signals at the specified *j*, which ranged from 0.0 to 2.2 A cm⁻², the OCP decay transient was recorded with a data collection interval of 0.2 ms for 1 s. The local pH was calculated using Eqn. (1) with the OCP value measured at 20 ms after the potential transient to OCP.

$$\text{Local pH} = E_{\text{OCP @ 20 ms}} (V_{\text{SHE}}) / -0.070 (@ 80 \text{ }^\circ\text{C}) \quad \text{Eqn. (1)}$$

Physical characterizations

SEM and EDS analyses were performed at an accelerating voltage of 5 and 15 kV, respectively, using a HITACHI S-4800. For cross-sectional SEM and EDS analyses, PTL samples were prepared by immersion in liquid N₂ followed by cutting. The noble metal contents on the modified Ti PTLs were measured using an X-ray fluorescence spectrometer (SIMULTIX12; RIGAKU).

Computational modeling

A computational modeling framework was developed using MATLAB to analyse the dynamic behaviour of Ti PTL dissolution, described by a system of conditional ordinary differential

equations. These equations model the concentration changes of ions and predict the real-time Ti dissolution profile, thereby introducing nonlinear dynamics. The “ode45” solver in MATLAB 2023a was employed for its robust handling of both stiff and non-stiff ordinary differential equation systems, ensuring accurate simulations across varied parameter sets. To refine the model and align it with experimental observations, genetic algorithm optimization was utilized to adjust the kinetic parameters, aiming to minimize the discrepancy between the predictions and experimental data.

Author contributions

Junsic Cho: Formal analysis, Investigation, Visualization, Writing - Original Draft, **Dong Hyun Kim:** Formal analysis, Investigation, Visualization, Writing - Original Draft, **Min Wook Noh:** Validation, **Haesol Kim:** Methodology, **Hong-Gyun Oh:** Resources, **Pilyoung Lee:** Resources, **Soobin Yoon:** Investigation, **Wangyun Won:** Investigation, **Young-June Park:** Conceptualization, Project administration, Funding acquisition, **Ung Lee:** Formal analysis, Data Curation, Writing - Original Draft, **Chang Hyuck Choi:** Writing - Original Draft, Supervision, Project administration.

Conflicts of interest

There are no conflicts to declare.

Data availability

Data for this article are available at the Zenodo repository at <https://doi.org/10.5281/zenodo.13117968>

Acknowledgements

This research was supported by the National Research Foundation of Korea (NRF) grant funded by the Korea government (MSIT) (No. 2022M3H4A3A01083536 and 2022K1A4A7A04095890). This research was also supported by Hyundai Motor Group and Shinsung C&T.

References

1. S. Chu, Y. Cui and N. Liu, *Nature Materials*, 2017, **16**, 16-22.
2. S. E. Hosseini and M. A. Wahid, *Renewable and Sustainable Energy Reviews*, 2016, **57**, 850-866.
3. H. Jin, B. Ruqia, Y. Park, H. J. Kim, H.-S. Oh, S.-I. Choi and K. Lee, *Advanced Energy Materials*, 2021, **11**, 2003188.
4. M. Bonanno, K. M ller, B. Bensmann, R. Hanke-Rauschenbach, D. Aili, T. Franken, A. Chromik, R. Peach, A. T. S. Freiberg and S. Thiele, *Advanced Materials Technologies*, 2024, **9**, 2300281.
5. N. D. Tomashov, R. M. Altovsky and G. P. Chernova, *Journal of The Electrochemical Society*, 1961, **108**, 113.
6. O. Panchenko, E. Borgardt, W. Zwaygardt, F. J. Hackem ller, M. Bram, N. Kardjilov, T. Arlt, I. Manke, M. M ller, D. Stolten and W. Lehnert, *Journal of Power Sources*, 2018, **390**, 108-115.
7. J. K. Lee, C. H. Lee and A. Bazylak, *Journal of Power Sources*, 2019, **437**, 226910.



8. T. Schuler, J. M. Ciccone, B. Krentscher, F. Marone, C. Peter, T. J. Schmidt and F. N. Büchi, *Advanced Energy Materials*, 2020, **10**, 1903216.
9. T. L. Doan, H. E. Lee, S. S. H. Shah, M. Kim, C.-H. Kim, H.-S. Cho and T. Kim, *International Journal of Energy Research*, 2021, **45**, 14207-14220.
10. D. H. Jeon, S. Kim, M. Kim, C. Lee and H.-S. Cho, *Journal of Power Sources*, 2023, **553**, 232322.
11. T. Srour, K. Kumar, V. Martin, L. Dubau, F. Maillard, B. Gilles, J. Dillet, S. Didierjean, B. Amoury, T. D. Le and G. Maranzana, *International Journal of Hydrogen Energy*, 2024, **58**, 351-361.
12. C. Rakousky, U. Reimer, K. Wippermann, M. Carmo, W. Lueke and D. Stolten, *Journal of Power Sources*, 2016, **326**, 120-128.
13. A. Lim, H.-Y. Jeong, Y. Lim, J. Y. Kim, H. Y. Park, J. H. Jang, Y.-E. Sung, J. M. Kim and H. S. Park, *Science Advances*, 2021, **7**, eabf7866.
14. S. Cherevko, T. Reier, A. R. Zeradjanin, Z. Pawolek, P. Strasser and K. J. J. Mayrhofer, *Electrochemistry Communications*, 2014, **48**, 81-85.
15. M. van der Merwe, R. Garcia-Diez, L. Lahn, R. E. Wibowo, J. Frisch, M. Gorgoi, W. Yang, S. Ueda, R. G. Wilks, O. Kasian and M. Bär, *ACS Catalysis*, 2023, **13**, 15427-15438.
16. O. Kasian, T. Li, A. M. Mingers, K. Schweinar, A. Savan, A. Ludwig and K. Mayrhofer, *Journal of Physics: Energy*, 2021, **3**, 034006.
17. A. Lončar, D. Escalera-López, F. Ruiz-Zepeda, A. Hrnjić, M. Šala, P. Jovanović, M. Bele, S. Cherevko and N. Hodnik, *ACS Catalysis*, 2021, **11**, 12510-12519.
18. L. Lahn, A. M. Mingers, A. Savan, A. Ludwig and O. Kasian, *ChemElectroChem*, 2024, **11**, e202300399.
19. J.-P. B. Haraldsted, Z. Révay, R. Frydendal, A. Verdager-Casadevall, J. Rossmeisl, J. Kibsgaard and I. Chorkendorff, *Materials Today Energy*, 2019, **14**, 100352.
20. Q. Xu, S. Z. Oener, G. Lindquist, H. Jiang, C. Li and S. W. Boettcher, *ACS Energy Letters*, 2021, **6**, 305-312.
21. C. Rakousky, U. Reimer, K. Wippermann, S. Kuhri, M. Carmo, W. Lueke and D. Stolten, *Journal of Power Sources*, 2017, **342**, 38-47.
22. J. C. Fornaciari, L.-C. Weng, S. M. Alia, C. Zhan, T. A. Pham, A. T. Bell, T. Ogitsu, N. Danilovic and A. Z. Weber, *Electrochimica Acta*, 2022, **405**, 139810.
23. S. Liu, I. Zaharieva, L. D'Amaro, S. Mebs, P. Kubella, F. Yang, P. Beyer, M. Haumann and H. Dau, *Advanced Energy Materials*, 2022, **12**, 2202914.
24. M. Pourbaix, *Atlas of Electrochemical Equilibria in Aqueous Solutions*, National Association of Corrosion Engineers, 1974.
25. E. R. Sauvė, B. Y. Tang, N. K. Razdan, W. L. Toh, S. Weng and Y. Surendranath, *Joule*, 2024, **8**, 728-745.
26. V. Kozlov, N. Bunkin, I. Ps, A. Shkirin, S. Zakharov and Z. Aa, *Water*, 2013, **4**, 129-154.
27. S. A. Berlinger, B. D. McCloskey and A. Z. Weber, *The Journal of Physical Chemistry B*, 2018, **122**, 7790-7796.
28. Y. Fovet, J.-Y. Gal and F. Toumelin-Chemla, *Talanta*, 2001, **53**, 1053-1063.
29. J.-F. Vanhumbecq and J. Proost, *Corrosion Reviews*, 2009, **27**, 117-204.
30. L. Fiedler, T.-C. Ma, B. Fritsch, J. H. Risse, M. Lechner, D. Dworschak, M. Merklein, K. J. J. Mayrhofer and A. Hutzler, *ChemElectroChem*, 2023, **10**, e202300373.
31. R. Srinivasan and F. Fasmin, *An introduction to electrochemical impedance spectroscopy*, CRC Press, 2021.
32. C. Liu, M. Carmo, G. Bender, A. Everwand, T. Lickert, J. L. Young, T. Smolinka, D. Stolten and W. Lehnert, *Electrochemistry Communications*, 2018, **97**, 96-99.
33. C. Liu, M. Shviro, A. S. Gago, S. F. Zaccarine, G. Bender, P. Gazdzicki, T. Morawietz, I. Biswas, M. Rasinski, A. Everwand, R. Schierholz, J. Pfeilsticker, M. Müller, P. P. Lopes, R.-A. Eichel, B. Pivovar, S. Pylypenko, K. A. Friedrich, W. Lehnert and M. Carmo, *Advanced Energy Materials*, 2021, **11**, 2002926.
34. T. L. Doan, T. N. Nguyen, Y. S. Jung, C. Lee, M. Kim, S. Lee, H.-S. Cho and T. Kim, *International Journal of Hydrogen Energy*, 2024, **55**, 839-847.
35. C. Rakousky, G. P. Keeley, K. Wippermann, M. Carmo and D. Stolten, *Electrochimica Acta*, 2018, **278**, 324-331.
36. S. Cherevko, S. Geiger, O. Kasian, A. Mingers and K. J. J. Mayrhofer, *Journal of Electroanalytical Chemistry*, 2016, **774**, 102-110.
37. O. Kasian, J.-P. Grote, S. Geiger, S. Cherevko and K. J. J. Mayrhofer, *Angewandte Chemie International Edition*, 2018, **57**, 2488-2491.
38. S. Cherevko, A. A. Topalov, A. R. Zeradjanin, G. P. Keeley and K. J. J. Mayrhofer, *Electrocatalysis*, 2014, **5**, 235-240.
39. A. A. Topalov, S. Cherevko, A. R. Zeradjanin, J. C. Meier, I. Katsounaros and K. J. J. Mayrhofer, *Chemical Science*, 2014, **5**, 631-638.
40. M. Zlatar, D. Escalera-López, M. G. Rodríguez, T. Hrbek, C. Götz, R. Mary Joy, A. Savan, H. P. Tran, H. N. Nong, P. Pobedinskas, V. Briega-Martos, A. Hutzler, T. Böhm, K. Haenen, A. Ludwig, I. Khalakhan, P. Strasser and S. Cherevko, *ACS Catalysis*, 2023, **13**, 15375-15392.
41. S. Cherevko, *Current Opinion in Electrochemistry*, 2018, **8**, 118-125.
42. S. A. Grigoriev, D. G. Bessarabov and A. S. Glukhov, *Russian Journal of Electrochemistry*, 2017, **53**, 808-812.
43. Q. Feng, X. Z. Yuan, G. Liu, B. Wei, Z. Zhang, H. Li and H. Wang, *Journal of Power Sources*, 2017, **366**, 33-55.
44. C. Liu, K. Wippermann, M. Rasinski, Y. Suo, M. Shviro, M. Carmo and W. Lehnert, *ACS Applied Materials & Interfaces*, 2021, **13**, 16182-16196.
45. C. Liu, J. A. Wrubel, E. Padgett and G. Bender, *Applied Energy*, 2024, **356**, 122274.
46. J. Cho, T. Lim, H. Kim, L. Meng, J. Kim, S. Lee, J. H. Lee, G. Y. Jung, K.-S. Lee, F. Viñes, F. Illas, K. S. Exner, S. H. Joo and C. H. Choi, *Nature Communications*, 2023, **14**, 3233.

